



**HAL**  
open science

## Structural Dynamics and Generalized Continua. In : Mechanics of Generalized Continua

Céline Chesnais, Claude Boutin, Stéphane Hans

► **To cite this version:**

Céline Chesnais, Claude Boutin, Stéphane Hans. Structural Dynamics and Generalized Continua. In : Mechanics of Generalized Continua. Structural Dynamics and Generalized Continua. In : Mechanics of Generalized Continua, SPRINGER, pp. 57-76, 2011, Advanced Structured Materials, 10.1007/978-3-642-19219-7\_3 . hal-00877882

**HAL Id: hal-00877882**

**<https://hal.science/hal-00877882>**

Submitted on 29 Oct 2013

**HAL** is a multi-disciplinary open access archive for the deposit and dissemination of scientific research documents, whether they are published or not. The documents may come from teaching and research institutions in France or abroad, or from public or private research centers.

L'archive ouverte pluridisciplinaire **HAL**, est destinée au dépôt et à la diffusion de documents scientifiques de niveau recherche, publiés ou non, émanant des établissements d'enseignement et de recherche français ou étrangers, des laboratoires publics ou privés.

# Structural Dynamics and Generalized Continua

Chesnais C., Boutin C. and Hans S.

*Published in “Mechanics of Generalized Continua”  
edited by H. Altenbach, G.A. Maugin and V. Erofeev,  
Advanced Structured Materials vol. 7, 2011.  
The original publication is available at  
[www.springerlink.com](http://www.springerlink.com)*

**Abstract** This paper deals with the dynamic behavior of reticulated beams made of the periodic repetition of symmetric unbraced frames. Such archetypical cells can present a high contrast between shear and compression deformabilities, conversely to “massive” media. This opens the possibility of enriched local kinematics involving phenomena of global rotation, inner deformation or inner resonance, according to studied configuration and frequency range. Firstly, the existence of these atypical behaviors is established theoretically through the homogenization method of periodic discrete media. Then, the results are adapted to buildings and confirmed with a numerical example.

**Key words:** Dynamics, discrete structure, periodic homogenization, local resonance, atypical modes, building, frame, shear wall

## 1 Introduction

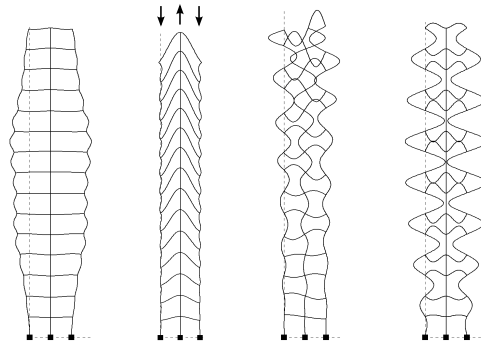
This paper deals with the macroscopic dynamic behavior of periodic reticulated structures widely encountered in mechanical engineering. Periodic lattices have been studied through various approaches [14] such as transfer matrix, variational approach [11], finite difference operator. Asymptotic methods of homogenization [16] initially developed for periodic media, were extended to multiple parameters and scale changes by [8] and adapted to periodic discrete structures by [4], then [12].

---

Chesnais C.  
Université Paris-Est, IFSTTAR, GER, F-75732, Paris, France,  
e-mail: [celine.chesnais@ifsttar.fr](mailto:celine.chesnais@ifsttar.fr)

Boutin C. and Hans S.  
DGCB, FRE CNRS 3237, École Nationale des Travaux Publics de l'État, Université de Lyon  
e-mail: [claude.boutin@entpe.fr](mailto:claude.boutin@entpe.fr); [stephane.hans@entpe.fr](mailto:stephane.hans@entpe.fr)

**Fig. 1** Examples of atypical normal modes of reticulated structures



Unbraced frame-type structures have also been considered in structural dynamics. The first studies focused on an individual bracing element such as a frame or coupled shear walls [17, 1]. Then the models were extended to the whole building [18, 15] and to 3D problems with torsion [15, 13]. All those methods aim to relate the features of the basic cell and the global behavior.

The morphology of reticulated beams is such that the basic cells can present a high contrast between shear and compression deformabilities (conversely to “massive” beams). This opens the possibility of enriched local kinematics involving phenomena of global rotation, inner deformation or inner resonance, according to studied configuration and frequency range [9, 6]. A numerical illustration of these atypical situations is given in Fig. 1 that shows some unusual macroscopic modes.

The present study investigates and summarizes those phenomena by a systematic analysis performed on the archetypical case of symmetric unbraced frame-type cells [2, 9, 5]. Assuming the cell size is small compared to the wavelength, the homogenization method of periodic discrete media leads to the macro-behavior at the leading order.

The paper is organized as follows. Section 2 gives an overview of the method and the assumptions. In Sect. 3, the studied structures are presented. Section 4 summarizes the various generalized beam models which can describe the transverse vibrations according to the properties of the basic cell elements and the frequency range. Section 5 is devoted to longitudinal vibrations and the effect of local resonance. Finally Sect. 6 explains how the results obtained for this particular class of structures can be generalized to more complex reticulated structures, for instance buildings. It is illustrated by a numerical example.

## 2 Overview of Discrete Homogenization

The analysis of periodic lattices of interconnected beams is performed in two steps [19]: first, the discretization of the balance of the structure under harmonic vibra-

tions; second, the homogenization, leading to a continuous model elaborated from the discrete description. An outline of this method is given hereafter.

**Discretization of the Dynamic Balance:** Studied structures (Fig. 2) are made of plates behaving like Euler-Bernoulli beams in out-of-plane motion, and assembled with rigid connections. The motions of each extremity connected to the same node are identical and define the discrete nodal kinematic variables of the system. The discretization consists in integrating the dynamic balance (in harmonic regime) of the beams, the unknown displacements and rotations at their extremities being taken as boundary conditions. Forces applied by an element on its extremities are then expressed as functions of the nodal variables. The balance of each element being satisfied, it remains to express the balance of forces applied to the nodes. Thus, the balance of the whole structure is rigorously reduced to the balance of the nodes.

**Homogenization Method:** The key assumption of homogenization is that the cell size in the direction of periodicity  $\ell_w$  is small compared to the characteristic size  $L$  of the vibrations of the structure. Thus  $\varepsilon = \ell_w/L \ll 1$ . The existence of a macro scale is expressed by means of macroscopic space variable  $x$ . The unknowns are continuous functions of  $x$  coinciding with the discrete variables at any node, e.g.  $U_\varepsilon(x = x_n) = U(\text{node } n)$ . These quantities, assumed to converge when  $\varepsilon$  tends to zero, are expanded in powers of  $\varepsilon$ :  $U_\varepsilon(x) = U^0(x) + \varepsilon U^1(x) + \varepsilon^2 U^2(x) + \dots$ . Similarly, all other unknowns, including the modal frequency, are expanded in powers of  $\varepsilon$ . As  $\ell_w = \varepsilon L$  is a small increment with respect to  $x$ , the variations of the variables between neighboring nodes are expressed using Taylor's series; this in turn introduces the macroscopic derivatives.

To account properly for the local physics, the geometrical and mechanical characteristics of the elements are scaled according to the powers of  $\varepsilon$ . As for the modal frequency, scaling is imposed by the balance of elastic and inertia forces at macro level. This scaling insures that each mechanical effect appears at the same order whatever the  $\varepsilon$  value is. Therefore, the same physics is kept when  $\varepsilon \rightarrow 0$ , i.e. for the homogenized model. Finally, the expansions in  $\varepsilon$  powers are introduced in the nodal balances. Those relations, valid for any small  $\varepsilon$ , lead for each  $\varepsilon$ -order to balance equations which describe the macroscopic behavior.

**Local Quasi-Static State and Local Dynamics:** In general the scale separation requires wavelengths of the compression and bending vibrations generated in each local element to be much longer than the element length at the modal frequency of the global system. In that case the nodal forces can be developed in Taylor's series with respect to  $\varepsilon$ . This situation corresponds to a quasi-static state at the local scale. Nevertheless, in higher frequency range, it may occur that only the compression wavelength is much longer than the length of the elements while local resonance in bending appears. The homogenization remains possible through the expansions of the compression forces and leads to atypical descriptions with inner dynamics. Above this frequency range, the local resonance in both compression and bending makes impossible the homogenization process.

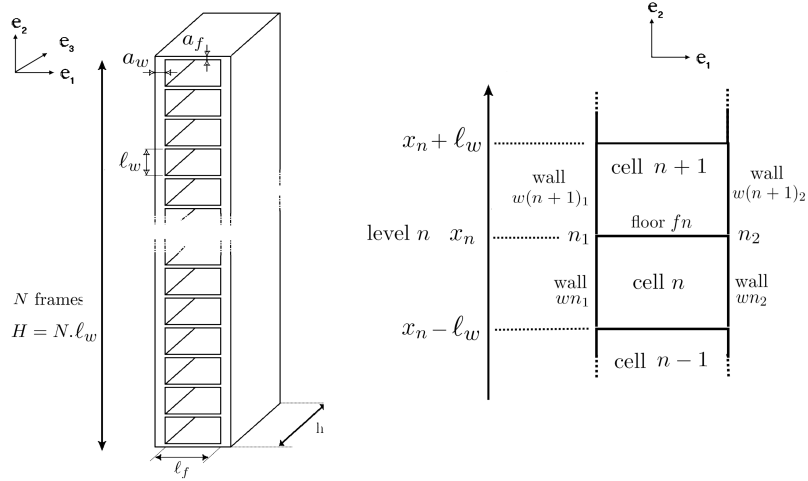


**Fig. 2** The class of studied structures (left) and the basic frame and notations (right)

### 3 Studied Structures

We study the vibrations of structures of height  $H = N \times \ell_w$  constituted by a pile of a large number  $N$  of identical unbraced frames called cells and made of a floor supported by two walls (Fig. 2). The parameters of floors ( $i = f$ ) and walls ( $i = w$ ) are: length  $\ell_i$ ; thickness  $a_i$ ; cross-section area  $A_i$ ; second moment of area  $I_i = a_i^3 h / 12$  in direction  $\mathbf{e}_3$ ; density  $\rho_i$ ; elastic modulus  $E_i$ .

The kinematics is characterized at any level  $n$  by the motions of the two nodes in the plane  $(\mathbf{e}_1, \mathbf{e}_2)$ , i.e., the displacements in the two directions and the rotation  $(u_1, u_2, \theta)$ . These six variables can be replaced by (cf. Fig. 3):

- Three variables associated to the rigid body motion of the level  $n$ : the mean transverse displacements,  $U(n)$  along  $\mathbf{e}_1$  and  $V(n)$  along  $\mathbf{e}_2$ , and the global rotation  $\alpha(n)$  (differential vertical nodal motion divided by  $\ell_f$ ),
- Three variables corresponding to its deformation: the mean and differential rotations of the nodes,  $\theta(n)$  and  $\Phi(n)$ , and the transverse dilatation  $\Delta(n)$ .

Because of the longitudinal symmetry, the transverse and longitudinal kinematics, respectively governed by  $(U, \alpha, \theta)$  and  $(V, \Phi, \Delta)$ , are uncoupled.

A systematic study enables to identify the family of possible dynamic behaviors by changing gradually the properties of the frame elements and the frequency range.

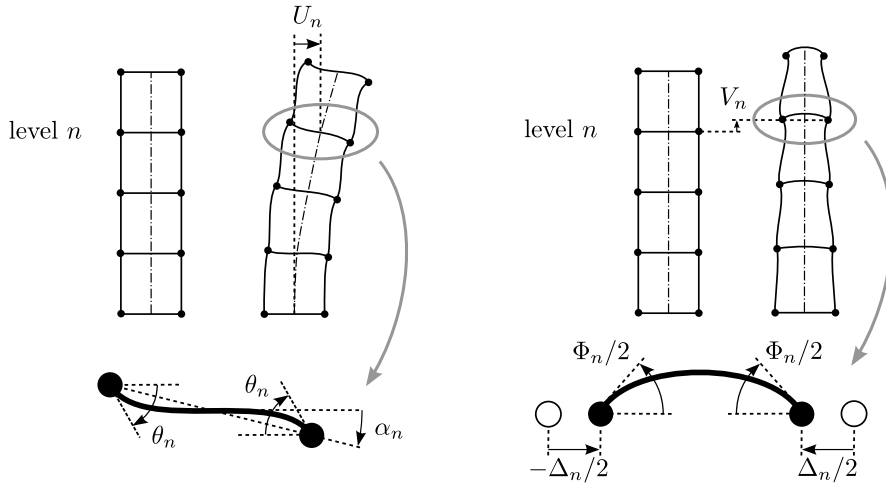


Fig. 3 Decoupling of transverse (left) and longitudinal (right) kinematics

## 4 Transverse Vibrations

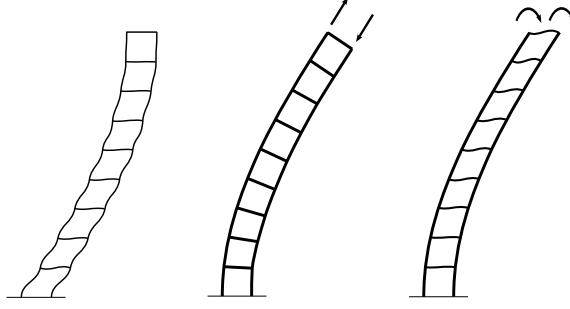
The transverse vibrations can be classified in two categories according to the nature of the governing dynamic balance. For the first category, the horizontal elastic forces balance the horizontal translation inertia. This corresponds to the “natural” transverse vibration modes presented in Sect. 4.1. It can be shown that the associated frequency range is such that the elements behave quasi-statically at the local scale (for lower frequencies, a static description of the structure is obtained). For the second category, the global elastic moment is balanced by the global rotation inertia. This leads to unusual gyration modes investigated in Sect. 4.3. This situation occurs at higher frequencies and local dynamics can appear.

### 4.1 “Natural” Transverse Vibrations: Translation Modes

The possible beam-like behaviors were established by varying the properties of the basic frame elements in [9] to which one may refer for a precise analysis. Here below the generic beam model derived from this approach is presented and an example devoted to a given type of cell frame is discussed.

The synthesis of the different macroscopic behaviors shows that only three mechanisms — shear, global bending, inner bending — govern the physics at the macroscale (Fig 4). Each of them is associated to a stiffness: in shear  $K$ , in global bending  $E_w I$ , and in inner bending  $E_w \mathcal{I}$ . The parameter  $I$  is the effective global bending inertia and  $\mathcal{I}$  is the effective inner bending inertia. Owing to the quasi-static local state, these parameters are deduced from the elastic properties of ele-

**Fig. 4** The three transverse mechanisms  
(left: shear,  
middle: global bending,  
right: inner bending)



ments in statics. For structures as in Fig. 2, they read ( $\Lambda$  stands for the linear mass):

$$K^{-1} = K_w^{-1} + K_f^{-1} \quad \text{with} \quad K_w = 24 \frac{E_w I_w}{\ell_w^2} \quad \text{and} \quad K_f = 12 \frac{E_f I_f}{\ell_w \ell_f} \quad (1a)$$

$$I = \frac{A_w \ell_f^2}{2} \quad ; \quad \mathcal{I} = 2 I_w \quad (1b)$$

$$\Lambda = \Lambda_w + \Lambda_f \quad \text{with} \quad \Lambda_w = 2 \rho_w A_w \quad \text{and} \quad \Lambda_f = \rho_f A_f \frac{\ell_f}{\ell_w} \quad (1c)$$

A generic beam model is built in order to involve the three mechanisms. It is governed by:

- Three beam constitutive laws relating the kinematic variables to (i) the macroscopic shear force  $T$ , (ii) the global bending moment  $M$  and (iii) the inner bending moment  $\mathcal{M}$ :

$$T = -K(U' - \alpha) \quad ; \quad M = -E_w I \alpha' \quad ; \quad \mathcal{M} = -E_w \mathcal{I} U'' \quad (2)$$

- The force and moment of momentum balance equations:

$$\begin{cases} (T - \mathcal{M}')' = \Lambda \omega^2 U \\ M' + T = 0 \end{cases} \quad (3)$$

It is worth noticing that the macroscopic behavior depends only on two kinematic variables:  $U$  and  $\alpha$  which describe the rigid body motion of the cross-section. The third variable associated to the transverse kinematics  $\theta$  has the status of a “hidden” internal variable which can be derived from the two other “driving” variables. The distinction between “driving” and “hidden” variables enables to generalize models built for the structures as in Fig. 2 to more complicated frame-type structures. Indeed, the implementation of the homogenization method of periodic discrete media on structures with three walls shows that the additional kinematic variables are “hidden” variables and that the macroscopic behavior is still described by (2) and (3). However expressions (1) which give the macroscopic parameters have to be modified. Their calculation in the general case is the subject of Sect. 6.2.

The generalized beam description presented above includes the three mechanisms but they do not have necessarily the same importance. The dominating effect(s) that actually drive(s) the effective behavior of a given structure can be identified through a dimensional analysis. In this aim, we introduce the characteristic size of vibration for the first mode  $\tilde{L} = 2H/\pi$  (for the  $n$ th mode of a clamped-free beam the characteristic size is  $\tilde{L}_n = 2H/[(2n-1)\pi]$ ). Moreover, the variables are rewritten as  $U = U^r U^*$  and  $\alpha = \alpha^r \alpha^*$  where the superscript  $r$  denotes reference values, and a  $*$  denotes the dimensionless terms,  $O(1)$  by construction. Introducing the expressions of the beam efforts (2) and making the change of variable  $\mathbf{x} = x/\tilde{L}$ , the set (3) becomes:

$$\begin{cases} \Omega^2 U^* + U^{*(2)} - C \gamma U^{*(4)} = (L \alpha^r / U^r) \alpha^{*f} \\ \alpha^* - C \alpha^{*(2)} = (U^r / L \alpha^r) U^{*f} \end{cases} \quad (4)$$

where superscripts in brackets stand for the order of derivative. The dimensionless numbers  $C$ ,  $\gamma$  and  $\Omega^2$  compare respectively global bending and shear, inner and global bendings, translation inertia and shear. They read:

$$C = \frac{E_w I}{K \tilde{L}^2} \quad ; \quad \gamma = \frac{\mathcal{J}}{I} \quad ; \quad \Omega^2 = \frac{\Lambda \omega^2 \tilde{L}^2}{K} \quad (5)$$

Eliminating  $\alpha^*$  (or  $U^*$ ) in (4) gives the differential equation governing  $U^*$  (or  $\alpha^*$ ):

$$C \gamma U^{*(6)} - (1 + \gamma) U^{*(4)} - \Omega^2 U^{*(2)} + \frac{\Omega^2}{C} U^* = O(\tilde{\epsilon}) \quad (6)$$

The term  $O(\tilde{\epsilon})$  highlights the fact that (6) is a zero-order balance and hence is only valid up to the accuracy  $\tilde{\epsilon}$ . Consequently, according to the values of  $C$ ,  $C \gamma$  and  $\gamma$  compared to  $\tilde{\epsilon}$  powers ( $\tilde{\epsilon} = \ell_w/\tilde{L} = \pi/(2N)$ ), equation (6) degenerates into simplified forms. The mapping (Fig. 5) gives the validity domain of the seven possible behaviors according to the two parameters  $x$  and  $y$  defined by  $C = \tilde{\epsilon}^x$  and  $\gamma = \tilde{\epsilon}^y$ . Note that, as the validity of the model requires the scale separation i.e.  $\ell_w/\tilde{L}_n < 1$ , the maximum number of homogenizable modes of a structure of  $N$  cells is  $n_{max} = N/3$ .

## 4.2 An Example: Slender Timoshenko Beam

Consider structures for which  $C = O(1)$  and  $\gamma \leq O(\tilde{\epsilon})$ . Then the terms related to  $C \gamma$  and  $\gamma$  are negligible in (6) and the generic beam degenerates into a slender Timoshenko beam driven by:

$$U^{*(4)} + \Omega^2 U^{*(2)} - \frac{\Omega^2}{C} U^* = O(\tilde{\epsilon}) \quad (7)$$

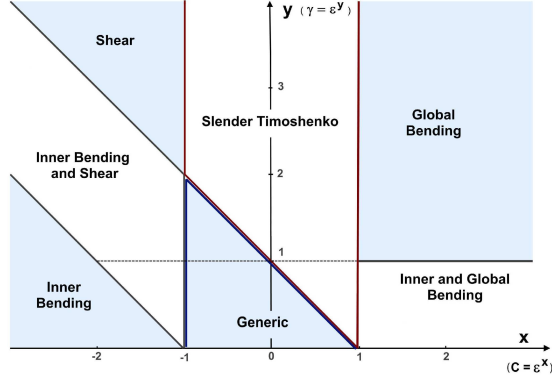


**Fig. 5** Map of different kinds of transverse “natural” behaviors in function of the parameters  $C = \varepsilon^x$  and  $\gamma = \varepsilon^y$ , [9]

To illustrate how to reach (7) by homogenization, consider a structure as in Fig. 2 with floors thicker than walls:

$$\frac{a_w}{l_w} = O(\varepsilon) \quad ; \quad \frac{a_f}{l_w} = O(\sqrt{\varepsilon}) \quad ; \quad \frac{\ell_w}{\ell_f} = O(1) \quad ; \quad \frac{E_w}{E_f} = O(1) \quad (8)$$

so that  $\Lambda = O(\Lambda_f)$ ,  $K = O(K_w)$  and, as required:

$$C = \frac{E_w I}{K_w \tilde{L}^2} = O\left(\frac{\ell_w^2 \ell_f^2}{a_w^2 \tilde{L}^2}\right) = O(1) \quad ; \quad \gamma = \frac{2 I_w}{I} = O\left(\frac{a_w^2}{\ell_f^2}\right) = O(\varepsilon^2) \quad (9)$$

The dynamic regime is reached when  $\Omega^2/C = O(1)$  i.e., accounting for  $C = O(1)$ , when the leading order of the circular frequency is:

$$\omega_0 = O(\tilde{L}^{-1} \sqrt{K_w/\Lambda_f}) = O(K_w/\sqrt{E_w I \Lambda_f})$$

In that case, the leading order equations obtained by homogenization are:

$$-K_w (U^{0''} - \theta^{0'}) = \Lambda_f \omega_0^2 U^0 \quad (10a)$$

$$K_f (\alpha^0 - \theta^0) = 0 \quad (10b)$$

$$-E_w I \alpha^{0''} - K_w (U^{0'} - \theta^0) = 0 \quad (10c)$$

Equation (10a) expresses the balance of horizontal forces at the leading order, while (10b) and (10c) come from the balance of both local and global moments at the first two significant orders. Equation (10b) also describes the inner equilibrium of the cell and imposes the node rotation  $\theta^0$  to be equal to the section rotation  $\alpha^0$ . Thus the macroscopic behavior is described by a differential set that governs the mean transverse motion  $U^0$  and the section rotation  $\alpha^0$ :

$$\begin{cases} -K_w (U^{0''} - \alpha^{0'}) = \Lambda_f \omega_0^2 U^0 \\ -E_w I \alpha^{0''} - K_w (U^{0'} - \alpha^0) = 0 \end{cases} \quad (11)$$

Eliminating  $\alpha^0$  provides: 
$$E_w I U^{0(4)} + \frac{E_w I}{K_w} \Lambda_f \omega^2 U^{0(2)} - \Lambda_f \omega_0^2 U^0 = 0$$

which corresponds to (7), i.e. a degenerated form of (6) with  $\gamma \leq O(\tilde{\varepsilon})$ .

The similarity with Timoshenko beams is obvious when rewriting (11) with the macro shear force  $\tilde{T}^0$  and the global bending moment  $\tilde{M}^0$  defined in (2) (here with  $^0$  superscript):

$$\begin{cases} T^{0'} = \Lambda_f \omega_0^2 U^0 \\ M^{0'} + T^0 = 0 \end{cases} \quad (12)$$

Two features distinguish (12) from the usual Timoshenko description of “massive” beams. First, the shear effect (that comes from the bending of the walls in parallel, see (1a)) remains at the leading order even if the reticulated structure is slender. Second, while the translation inertia is significant in the force balance (12a), the rotation inertia is negligible in the moment balance (12b) (where the effective bending results from the opposite extension-compression of the two walls distant of the floor length). In other words, the translation is in dynamic regime but the rotation stays in quasi-static regime for the considered frequency range. This leads to investigate higher frequencies to obtain rotational dynamics.

### 4.3 Atypical Transverse Vibrations: Gyration Modes

This section is devoted to gyration modes, i.e. transverse modes governed by the section rotation  $\alpha$  (Fig.6). Their existence is first established on a particular case. Then the results are slightly generalized.

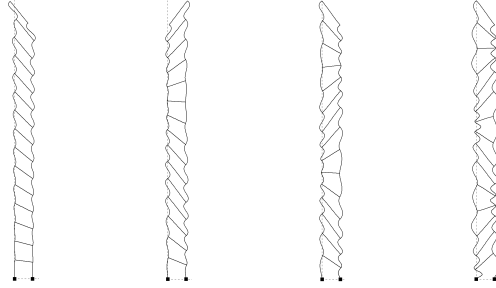


**Fig. 6** Examples of gyration modes

We come back to the structure studied in the previous section and whose geometry and parameters are scaled by (8). The frequency range is increased of one order in  $\varepsilon$ , i.e.  $\omega_0 = O(\ell_w^{-1} \sqrt{K_w/\Lambda_f})$  which remains sufficiently low to insure that the elements behave quasi-statically at the local scale. Then, the leading order equations obtained by homogenization become:

$$0 = \Lambda_f \omega_0^2 U^0 \quad (13a)$$

$$K_f (\alpha^0 - \theta^0) = 0 \quad (13b)$$

$$-E_w I \alpha^{0''} - K_w (U^{0'} - \theta^0) = \frac{\rho_f A_f \ell_f^3}{420 \ell_w} \omega_0^2 (42 \alpha^0 - 7 \theta^0) \quad (13c)$$

The comparison of (10) and (13) shows that the higher frequency leaves the inner equilibrium condition of the cell (13b) unchanged (thus, here also, the mean rotation of the nodes matches the section rotation, i.e.  $\theta^0 = \alpha^0$ ). Conversely, in (13a), the increased order of magnitude of inertia terms makes that  $\Lambda_f \omega_0^2 U^0$  cannot be balanced by horizontal elastic forces, thus the section translation vanishes at the leading order,  $U^0 = 0$ . In parallel, the rotation inertia now appears in the moment of momentum balance (13c). After eliminating  $\theta^0$ , the macroscopic behavior at the leading order is described by the following differential equation of the second degree:

$$\begin{aligned} -E_w I \alpha^{0''} + K_w \alpha^0 &= J_f \omega_0^2 \alpha^0 & (14) \\ \theta^0 = \alpha^0 \quad ; \quad U^0 = 0 \quad ; \quad J_f &= \frac{\rho_f A_f \ell_f^3}{12 \ell_w} \end{aligned}$$

This is an atypical gyration beam model fully driven by the section rotation  $\alpha^0$  without lateral translation (more precisely, one shows that the first non vanishing translation is of the second order  $\varepsilon^2 U^2 = (K_w / (\Lambda_f \omega_0^2)) \alpha^{0'}$ ). The gyration dynamics is governed by the mechanism of opposite traction-compression of vertical elements (whose elastic parameter is the global bending stiffness  $E_w I$ ), the shear of the cell (stiffness  $K_w$ ) acting as an inner elastic source of moment, and the rotation inertia of the thick floors ( $J_f$ ). Solutions of (14) (in  $\alpha^0$ ) have a classical sinusoidal expression but, due to the presence of the source term  $K_w \alpha^0$ , the frequency distribution is atypical.

Note that the thick floors of the specific studied frame lead to neglect the shear stiffness of the floors and the rotation inertia of the walls. The particular description (14) can be extended to other types of frames by considering the cell shear stiffness  $K$  instead of  $K_w$  and rotation inertia  $J$  instead of  $J_f$  (for structures as in Fig. 2,  $J = J_f + J_w$  with  $J_w = \rho_w A_w \ell_f^2 / 2$ ). Introducing the macroscopic shear force  $T^0$  and the global bending moment  $M^0$  already defined in (2) and accounting for  $U^0 = 0$  show that (14) is nothing but the moment of momentum balance of the usual Timoshenko formulation:

$$T^0 + M^{0'} = J_f \omega_0^2 \alpha^0 \quad (15)$$

However, in ‘‘massive’’ Timoshenko beams, variables  $U$  and  $\alpha$  reach the dynamic regime in the same frequency range, hence both are involved in common modes. Conversely, for the reticulated beams studied here, ‘‘natural’’ and gyration modes are uncoupled because the dynamic regimes for  $U$  and  $\alpha$  occur in different frequency ranges. This specificity implies that in the frequency range of non-homogenizable ‘‘natural’’ modes, it exists homogenizable gyration modes. For a detailed analysis of the conditions of existence of gyration modes, one may refer to [7].

Because gyration modes appear in a higher frequency domain than “natural” modes, the elements have not necessarily a quasi-static behavior at the local scale and phenomena of local dynamics can also occur. In this case, the bending wavelength in the elements is of the order of their length, whereas the compression wavelength remains much larger. This enables to expand the compression forces and to derive a macroscopic behavior. The governing equation of the second degree presents the same global moment parameter than for local quasi-static state but differs fundamentally by the inertia term and the inner elastic source of moment, both depending on frequency:

$$E_w I \alpha'' - K(\omega) \alpha + J(\omega) \omega^2 \alpha = 0 \quad (16)$$

The reason of these modifications lies in the non expanded bending forces that strongly depend on the frequency and that give rise to apparent inertia  $J(\omega)$  and moment source. This effect also appears in longitudinal vibrations and is discussed in the next section.

## 5 Longitudinal Vibrations

The longitudinal vibrations, described by  $(V, \Phi, \Delta)$ , present a lesser complexity because the main mechanism is the vertical compression. The difference between the identified models only relies in the possible presence of local dynamics.

**Local Quasi-Static State:** This case leads to the classical description of beam characterized by the compression modulus  $2 E_w A_w$  and the linear mass  $\Lambda$ :

$$2 E_w A_w V'' + \Lambda \omega^2 V = 0 \quad (17)$$

The domain of validity of this model is derived by expressing that the order of magnitude of the fundamental frequency of the whole structure (described by (17)) is much smaller than the one of the elements in bending. For structures whose walls and floors are made of the same material, a sufficient condition is to have a large number of cells:  $N \geq (\ell_i/a_i)$ .

**Local Dynamics:** Similarly to gyration modes, the local dynamics introduces a frequency depending apparent mass, that can be expressed analytically [6, 5]:

$$2 E_w A_w V'' + \Lambda(\omega) \omega^2 V(x) = 0 \quad (18a)$$

$$\Lambda(\omega) = \Lambda_w + \Lambda_f \frac{8}{3\pi \sqrt{\frac{\omega}{\omega_{f1}}} \left[ \coth\left(\frac{3\pi}{4} \sqrt{\frac{\omega}{\omega_{f1}}}\right) + \cot\left(\frac{3\pi}{4} \sqrt{\frac{\omega}{\omega_{f1}}}\right) \right]} \quad (18b)$$

The study of  $\Lambda(\omega)$  (cf. Fig. 7), shows that (i)  $\Lambda(\omega) \rightarrow \Lambda$  when  $\omega \rightarrow 0$ , and (ii)  $|\Lambda(\omega)| \rightarrow \infty$  when  $\omega \rightarrow \omega_{f(2k+1)}$ , where  $\omega_{f(2k+1)}$  are the circular frequencies of the odd normal modes of horizontal elements in bending. This induces abnormal re-

sponse in the vicinity of the  $\omega_{f(2k+1)}$  that results in discrete spectrum of frequency band gaps. Other frequency band gaps are generated by the excitation of modes of the walls or of the whole cell which blocks the global kinematics [5]. However this effect is described by higher order equations and, in a damped structure, it has probably less influence than the frequency band gaps of zero order.

## 6 Extension and Application to Buildings

Ordinary concrete buildings (as the one presented in Fig. 8) are very frequently made up of identical stories and their structure is periodic in height. Moreover, the experimental modal shapes suggest using continuous beam models to describe their first modes of vibration. For instance, Fig. 9 compares experimental data with the normal modes of a Timoshenko beam whose features were chosen in order to fit to the first two experimental frequencies [3, 10]. For these reasons we now propose to adapt the beam models derived in the previous sections to buildings. Such an approach presents two main advantages:

- The upscaling analysis provides a clear understanding of the dynamics of the structure.
- Calculations are greatly reduced since the dynamic analysis is performed on a 1D analytical model instead of the complete 3D numerical model of the building.

Applications concern as well preliminary design of new structures as seismic diagnosis and reinforcement of existing buildings.

As earthquakes principally shake the first “natural” transverse modes of buildings, the study focuses on the models of Sect. 4.1. The use of homogenized models requires the structure to respect some conditions. Firstly, the scale separation implies that the building should have at least  $N = 5$  stories and that the maximum number of studied modes in a given direction is  $n_{max} = N/3$ . Secondly, the structure should be symmetric to avoid coupling between the two transverse directions and torsion because the homogenized models describe motion in a plane. Moreover, the models were derived by assuming that elements behave like Euler-Bernoulli beams. This hypothesis is acceptable for structures with columns and beams but not for structures with shear walls. Therefore, we have to add the shear mechanism in the elements. This is the subject of Sect. 6.1. Next, the new model is applied to the building of Fig. 8 and the calculation of macroscopic parameters is explained (Sect. 6.2).

### 6.1 Generic Beam Model for Structures with Shear Walls

For the structures with thin columns studied in Sect. 4.1, “natural” transverse modes are governed by three mechanisms: shear, global bending and inner bending (Fig. 4). As the global bending results from the opposite extension-compression of the two

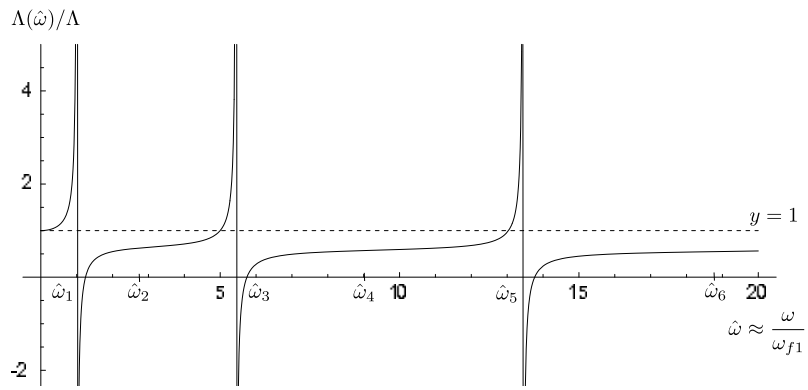


Fig. 7 Effect of the local resonance on the apparent dimensionless mass  $\Lambda(\hat{\omega})/\Lambda$  for  $\Lambda_w = \Lambda_f$

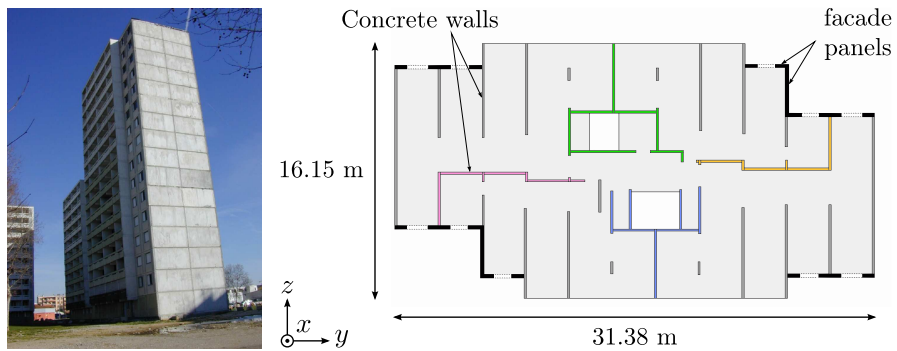
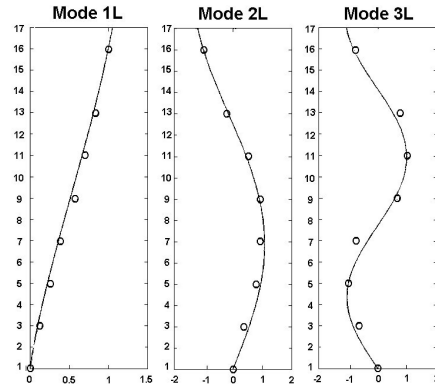


Fig. 8 Studied building and its typical floor plan view

Fig. 9 Comparison of experimental (circles) and Timoshenko (continuous lines) mode shapes in direction y. Only two parameters were used for the fitting of the Timoshenko beam: the first two experimental frequencies. (Experimental frequencies in Hz: 2.15 ; 7.24 ; 13.97 ; 20.5 - Timoshenko beam frequencies in Hz: 2.15 ; 7.24 ; 13.96 ; 20.1)



walls, its physics is unchanged by the increase of the wall thickness. On the contrary, shear and inner bending are generated by the bending of the elements at the local and the global scales respectively. Therefore the shear mechanism in the walls has now to be taken into account. For local bending, this effect is naturally included during the calculation of  $K$  the shear stiffness of the cell and it does not modify the beam models. This is not the case for the shear associated to the bending of the walls at the global scale which requires to add a fourth mechanism. Consequently, the generic beam model of Sect. 4.1 is valid as long as walls behave like Euler-Bernoulli beams *at the global scale*.

For structures with shear walls which do not respect the previous condition, a new model involving the four mechanisms is derived from the homogenization of the dynamic behavior of structures as in Fig. 2 by considering that the elements behave now like Timoshenko beams. To make the shear associated with inner bending emerge at the leading order, the wall geometry should respect:  $a_w/\ell_w \geq O(\varepsilon^{-1})$ . The new generic beam model is governed by:

- four beam constitutive laws relating the kinematic variables to (i) the shear force associated to the local bending of the floor  $T$ , (ii) the shear force associated to the shear in the walls  $\tau$ , (iii) the global bending moment  $M$  and (iv) the inner bending moment  $\mathcal{M}$ :

$$\begin{aligned} T &= -\mathcal{K}_f(\alpha - \theta) & M &= -E_w I \alpha' \\ \tau &= -\mathcal{K}_w(U' - \theta) & \mathcal{M} &= -E_w \mathcal{I} \theta' \end{aligned} \quad (19)$$

- three balance equations closed to (3):

$$\tau' = \Lambda \omega^2 U \quad ; \quad M' + T = 0 \quad ; \quad T - \mathcal{M}' = \tau \quad (20)$$

Combining (19) and (20) gives the sixth degree differential equation describing the macroscopic behavior of the structure:

$$\begin{aligned} \frac{E_w \mathcal{I} E_w I}{\mathcal{K}_f} U^{(6)} - \left( E_w \mathcal{I} + E_w I - \Lambda \omega^2 \frac{E_w \mathcal{I} E_w I}{\mathcal{K}_w \mathcal{K}_f} \right) U^{(4)} \\ - \left( \frac{E_w \mathcal{I}}{\mathcal{K}_w} + E_w I \left( \frac{1}{\mathcal{K}_w} + \frac{1}{\mathcal{K}_f} \right) \right) \Lambda \omega^2 U'' + \Lambda \omega^2 U = 0 \end{aligned} \quad (21)$$

The main differences with the model presented in Sect. 4.1 are listed below:

- The replacement of  $U''$  by  $\theta'$  in the constitutive law associated to inner bending,
- The distinction between the shear forces in the walls and in the floor,
- An additional balance equation (20c) which expresses the inner equilibrium of the cell.

As a result, (21) contains two new terms (in frame) which become negligible when the shear of the walls is much more rigid than inner bending ( $E_w \mathcal{I} \ll \mathcal{K}_w L^2$ ). Moreover, the three variables related to the transverse kinematics,  $U$ ,  $\alpha$  and  $\theta$ ,

emerge at the macroscopic scale. Therefore the generalization of this model to more complicated frame-type structures is an open question. However the implementation of the homogenization method on structures with three walls shows that this model is still valid when the three walls are identical. In the following we assume that this model is a good approximation of the behavior of structures with walls mechanical properties of which are not too different.

## 6.2 Calculation of Macroscopic Parameters

This section illustrates the relevance of the previous generalized beam model to describe the dynamic behavior of a 16-story building (Fig. 8) on which in situ measurements have been carried out. The structure is in reinforced concrete with pre-cast facade panels. In order to evaluate the accuracy of the beam models, the results are compared with full 3D finite element simulations (and eventually with the experimental data). The COMSOL Multiphysics software is used in the linear range. Floors and shear walls are represented by perfectly connected shells and the influence of facade panels is neglected. We make the number of stories vary between 6 and 30. Reinforced concrete properties are summarized below:

$$\begin{array}{ccc} \text{Density} & \text{Young's Modulus} & \text{Poisson's ratio} \\ \rho = 2300 \text{ kg/m}^3 & E = 30000 \text{ MPa} & \nu = 0.2 \end{array} \quad (22)$$

The use of the generic beam model of Sect. 6.1, which describes shear wall buildings, requires to calculate five macroscopic parameters: the linear mass which is equal to the mass of a story divided by the story height and the rigidities associated to the four mechanisms. The effective inertias of global and inner bendings are evaluated with formulas of the beam theory:

$$I = \sum_{\text{walls}} A_j d_j^2 \quad ; \quad \mathcal{I} = \sum_{\text{walls}} I_j \quad (23)$$

where  $A_j$  stands for the cross-section area and  $I_j$  for the second moment of area of wall  $j$ . The parameter  $d_j$  is the projection of the distance between the centroid of wall  $j$  and the centroid of all the walls onto the axis  $y$  or  $z$  (Fig 8) according to the studied direction.

It remains to estimate the two shear rigidities  $\mathcal{K}_f$  and  $\mathcal{K}_w$ . As the shape of the floor can be very complex, there is no analytical expression of  $\mathcal{K}_f$ . Thus, we propose to derive it from the shear rigidity of the whole cell  $K$  obtained thanks to a finite element modeling of one story. The boundary conditions are those identified by homogenization and are presented in Fig. 10. It consists in:

- preventing the rigid body motion of the cell by blocking both vertical and horizontal translations of a wall and the vertical translation of a second wall at the centroid of their lower cross-sections,

- imposing periodic boundary conditions between bottom and top of each wall,
- applying a distortion  $\Delta U/\ell$  where  $\ell = 2.70$  m is the story height,
- blocking the vertical translation of all the walls which is consistent with a global shear distortion.

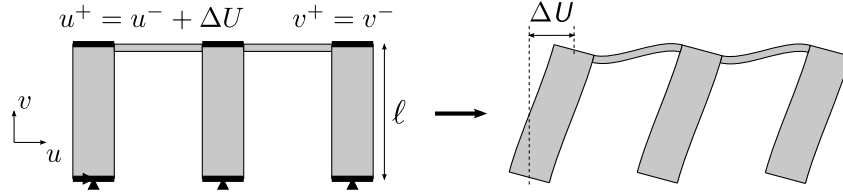


**Fig. 10** Boundary conditions for the calculation of the shear rigidity of the whole cell  $K$

Note that those boundary conditions allow the rotation of the walls. The shear rigidity of the whole cell  $K$  is derived from the calculated shear force in the walls. Then contributions of the floor  $\mathcal{K}_f$  and the walls  $\mathcal{K}_w$  are separated thanks to the formula obtained by homogenization for structures as in Fig. 2 (connection in series):

$$K = \frac{|\sum_{\text{walls}} T_j|}{\Delta U/\ell} \quad ; \quad \frac{1}{\mathcal{K}_f} = \frac{1}{K} - \frac{1}{\mathcal{K}_w} \quad (24)$$

According to the complexity of the walls, the shear rigidity  $\mathcal{K}_w$  is evaluated either with analytical expressions of the beam theory or with the finite element modeling of one story. In the latter case, the walls are clamped at their extremities, undergo a distortion (Fig. 11) and the shear rigidity is deduced from the calculated shear force.

$$\mathcal{K}_w = \sum_{\text{walls}} \kappa_j A_j G_j \quad \text{or} \quad \mathcal{K}_w = \frac{|\sum_{\text{walls}} T_j|}{\Delta U/\ell} \quad (25)$$

( $\kappa_j$ : Timoshenko shear coefficient,  $A_j$ : cross-section area and  $G_j$ : shear modulus)

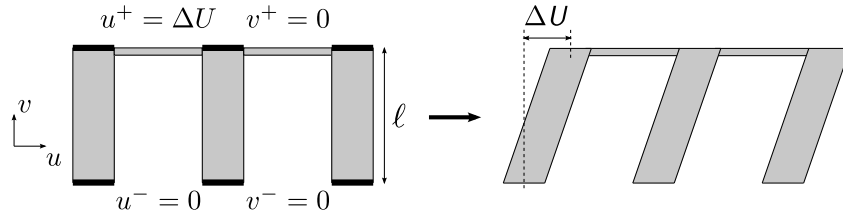


**Fig. 11** Boundary conditions for the calculation of the shear rigidity of the walls  $\mathcal{K}_w$

For the studied building, both shear rigidities were estimated with a finite element modeling. Figure 12 presents the deformation of one story due to the load

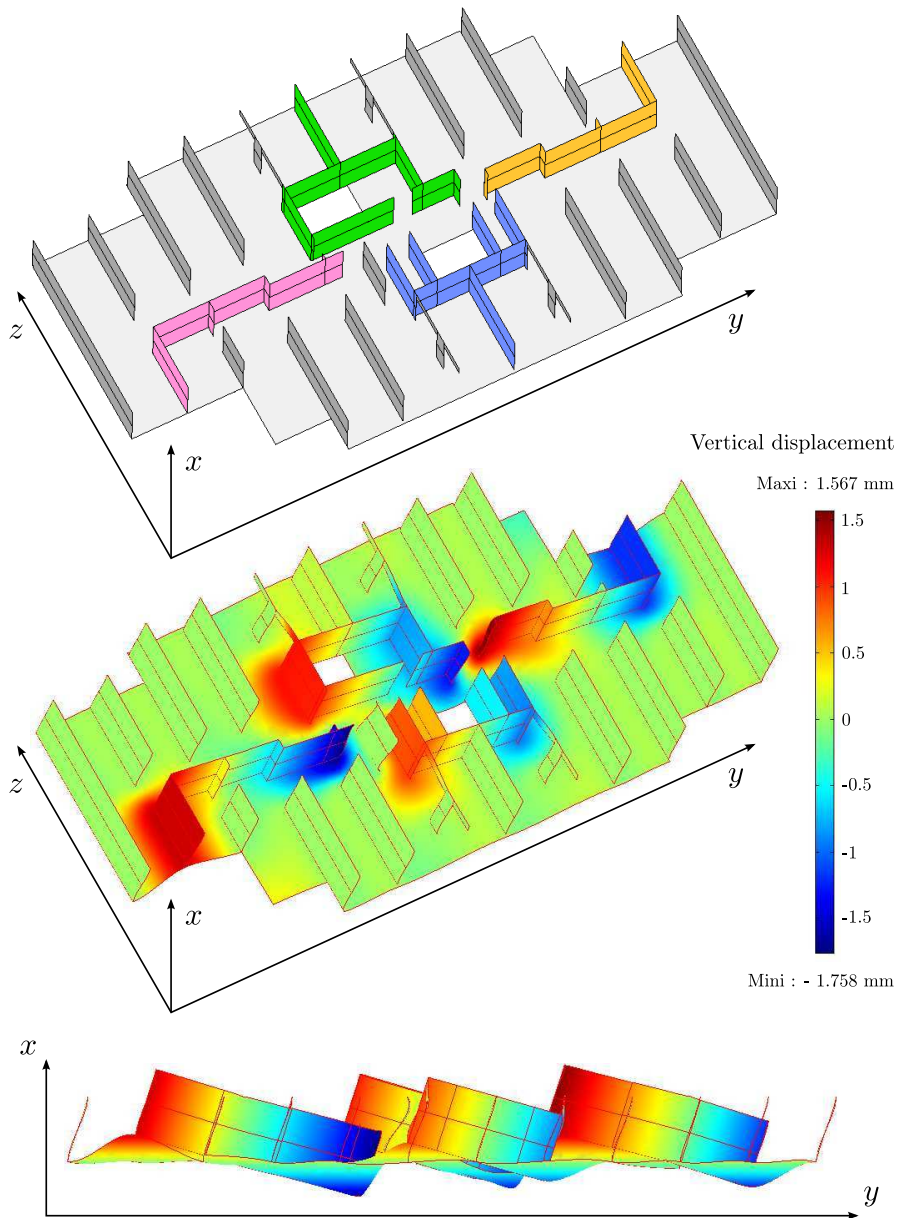


**Fig. 12** Finite element modeling of one story for the calculation of the shear rigidity of the cell  $K$  in direction  $y$ . Top: undeformed story, middle and bottom: deformed story.

applied for the calculation of the shear rigidity of the whole cell  $K$  in direction  $y$ . Note that the maximum vertical displacement is greater than the imposed horizontal distortion  $\Delta U = 1$  mm. The values of all the macroscopic parameters are given in Table 1 for direction  $y$ . The resonant frequencies calculated with a finite element modeling of the whole structure and with the generic beam models of Sects. 4.1 (column structure) and 6.1 (shear wall structure) are summarized in Table 2.

**Table 1** Values of macroscopic parameters for the studied building in direction  $y$

$\Lambda$ (t/m)	$I$ (m <sup>4</sup> )	$\mathcal{I}$ (m <sup>4</sup> )	$K$ (MN)	$\mathcal{K}_w$ (MN)	$\mathcal{K}_f$ (MN)
100	1648	56	7841	59056	9041

**Table 2** Resonant frequencies (in Hz) of the studied building in direction  $y$

Mode	Finite Elements		Generic beam of Sect. 4.1 (column structure)		Generic beam of Sect. 6.1 (shear wall structure)	
6 stories $\Rightarrow \varepsilon \approx 0.26$						
1	7.43		10.59	+ 42%	8.10	+ 9.0%
2	23.28		57.48	+ 147%	27.79	+ 19%
11 stories $\Rightarrow \varepsilon \approx 0.14$						
1	3.38		4.02	+ 19%	3.54	+ 4.6%
2	11.69		18.50	+ 58%	12.81	+ 9.6%
3	21.00		47.94	+ 128%	25.88	+ 23%
16 stories $\Rightarrow \varepsilon \approx 0.098$						
1	2.08	(2.15 <sup>a</sup> )	2.31	+ 11%	2.13	+ 2.2%
2	7.26	(7.25 <sup>a</sup> )	9.53	+ 31%	7.63	+ 5.1%
3	14.30	(14.00 <sup>a</sup> )	23.33	+ 63%	15.61	+ 9.2%
30 stories $\Rightarrow \varepsilon \approx 0.052$						
1	0.91		0.96	+ 5.4%	0.92	+ 1.4%
2	3.16		3.52	+ 11%	3.21	+ 1.5%
3	6.36		7.71	+ 21%	6.49	+ 2.0%

<sup>a</sup> Experimental frequencies

The generic beam model of Sect. 4.1 gives reasonable results for the first resonant frequencies when the number of stories is sufficiently high and walls behave like Euler-Bernoulli beams at the global scale. But, this model and then all its simplified forms are unsuitable for the higher modes and the structures with few stories. In these cases, the results are significantly improved by the use of the generic beam model of Sect. 6.1 which includes the shear in the walls. The estimated frequencies are very closed to the ones calculated by finite elements (and to the experimental

data), which shows that the physics of the problem has been taken into account with considerably reduced calculations.

## 7 Conclusion

At the macroscopic scale, unbraced (or weakly braced) reticulated structures present a much more complex behavior than usual “massive” media. It comes from the high contrast between shear and compression deformabilities which enables enriched local kinematics (gyration modes and inner bending mechanism) and phenomena of local resonance in bending. Consequently, there is an analogy between those structures and generalized media. The gyration beam model looks like Cosserat medium, structures where inner bending is not negligible are similar to micromorphic media and local resonance is a way to design metamaterials. Thanks to dimensional analysis, it is possible to extend these results to other types of structures of decametric size such as buildings but also of millimetric size such as foams or of nanometric size such as graphene tubes. Future works can as well deal with the other vibration modes which are governed by the inner deformation of the cell (Fig. 1).

**Acknowledgements** The authors thank Prof. Y. Debard for giving free access to the code RDM6.

## References

1. Basu, A.K., Nagpal, A.K., Bajaj, R.S., Guliani, A.K.: Dynamic characteristics of coupled shear walls. *J. Struct. Div.* **105**(8), 1637–1652 (1979)
2. Boutin, C., Hans, S.: Homogenisation of periodic discrete medium: Application to dynamics of framed structures. *Comput. Geotech.* **30**(4), 303–320 (2003)
3. Boutin, C., Hans, S., Ibrahim, E., Roussillon, P.: In situ experiments and seismic analysis of existing buildings. Part II: Seismic integrity threshold. *Earthq. Eng. Struct. Dyn.* **34**(12), 1531–1546 (2005)
4. Caillerie, D., Trompette, P., Verna, P.: Homogenisation of periodic trusses. In: *IASS Symposium, 10 Years of Progress in Shell and Spatial Structures*. Madrid (1989)
5. Chesnais, C.: *Dynamique de milieux réticulés non contreventés. Application aux bâtiments*. PhD thesis, ENTPE, Lyon (2010). [http://bibli.ec-lyon.fr/exl-doc/TH\\_T2177\\_cchesnais.pdf](http://bibli.ec-lyon.fr/exl-doc/TH_T2177_cchesnais.pdf)
6. Chesnais, C., Hans, S., Boutin, C.: Wave propagation and diffraction in discrete structures: Effect of anisotropy and internal resonance. *PAMM* **7**(1), 1090,401–1090,402 (2007)
7. Chesnais, C., Hans, S., Boutin, C.: Dynamics of reticulated structures: Evidence of atypical gyration modes. *Int. J. Multiscale Comput. Eng.* **9**(5), 515–528 (2011)
8. Cioranescu, D., Saint Jean Paulin, J.: *Homogenization of Reticulated Structures*, *Applied Mathematical Sciences*, vol. 136. Springer-Verlag, New York (1999)
9. Hans, S., Boutin, C.: Dynamics of discrete framed structures: A unified homogenized description. *J. Mech. Mater. Struct.* **3**(9), 1709–1739 (2008)
10. Hans, S., Boutin, C., Ibrahim, E., Roussillon, P.: In situ experiments and seismic analysis of existing buildings. Part I: Experimental investigations. *Earthq. Eng. Struct. Dyn.* **34**(12), 1513–1529 (2005)

11. Kerr, A.D., Accorsi, M.L.: Generalization of the equations for frame-type structures; a variational approach. *Acta Mech.* **56**(1-2), 55–73 (1985)
12. Moreau, G., Caillerie, D.: Continuum modeling of lattice structures in large displacement applications to buckling analysis. *Comput. Struct.* **68**(1-3), 181–189 (1998)
13. Ng, S.C., Kuang, J.S.: Triply coupled vibration of asymmetric wall-frame structures. *J. Struct. Eng.* **126**(8), 982–987 (2000)
14. Noor, A.K.: Continuum modeling for repetitive lattice structures. *Appl. Mech. Rev.* **41**(7), 285–296 (1988)
15. Potzta, G., Kollár, L.P.: Analysis of building structures by replacement sandwich beams. *Int. J. Solids Struct.* **40**(3), 535–553 (2003)
16. Sanchez-Palencia, E.: Non-homogeneous media and vibration theory, *Lecture notes in physics*, vol. 127. Springer-Verlag, Berlin (1980)
17. Skattum, K.S.: Dynamic analysis of coupled shear walls and sandwich beams. Rep. EERL 71-06 PhD thesis, California Institute of Technology (1971)
18. Stafford Smith, B., Kuster, M., Hoenderkamp, J.C.D.: Generalized method for estimating drift in high-rise structures. *J. Struct. Eng.* **110**(7), 1549–1562 (1984)
19. Tollenaere, H., Caillerie, D.: Continuous modeling of lattice structures by homogenization. *Adv. Eng. Softw.* **29**(7-9), 699–705 (1998)